Photoacoustics 8 (2017) 48–58

Contents lists available at ScienceDirect

Photoacoustics

journal homepage: www.elsevier.com/locate/pacs

Research article

Quantitative comparison of PZT and CMUT probes for photoacoustic imaging: Experimental validation

Maëva Vallet[a], François Varray[a,*], Jérôme Boutet[b], Jean-Marc Dinten[b], Giosuè Caliano[c], Alessandro Stuart Savoia[c], Didier Vray[a]

[a] Univ Lyon, INSA-Lyon, Université Lyon 1, UJM-Saint Etienne, CNRS, Inserm, CREATIS UMR 5220, U1206, F-69621 Lyon, France
[b] CEA-LETI, MINATEC, F-38054 Grenoble, France
[c] Dipartimento di Ingegneria, Università degli Studi Roma Tre, Rome, Italy

ARTICLE INFO

Article history:
Received 14 September 2016
Received in revised form 27 July 2017
Accepted 8 September 2017
Available online 22 September 2017

Keywords:
Photoacoustic
Ultrasound imaging
CMUT
PZT

ABSTRACT

Photoacoustic (PA) signals are short ultrasound (US) pulses typically characterized by a single-cycle shape, often referred to as N-shape. The spectral content of such wideband signals ranges from a few hundred kilohertz to several tens of megahertz. Typical reception frequency responses of classical piezoelectric US imaging transducers, based on PZT technology, are not sufficiently broadband to fully preserve the entire information contained in PA signals, which are then filtered, thus limiting PA imaging performance. Capacitive micromachined ultrasonic transducers (CMUT) are rapidly emerging as a valid alternative to conventional PZT transducers in several medical ultrasound imaging applications. As compared to PZT transducers, CMUTs exhibit both higher sensitivity and significantly broader frequency response in reception, making their use attractive in PA imaging applications. This paper explores the advantages of the CMUT larger bandwidth in PA imaging by carrying out an experimental comparative study using various CMUT and PZT probes from different research laboratories and manufacturers. PA acquisitions are performed on a suture wire and on several home-made bimodal phantoms with both PZT and CMUT probes. Three criteria, based on the evaluation of pure receive impulse response, signal-to-noise ratio (SNR) and contrast-to-noise ratio (CNR) respectively, have been used for a quantitative comparison of imaging results. The measured fractional bandwidths of the CMUT arrays are larger compared to PZT probes. Moreover, both SNR and CNR are enhanced by at least 6 dB with CMUT technology. This work highlights the potential of CMUT technology for PA imaging through qualitative and quantitative parameters.

1. Introduction

Photoacoustic imaging (PAI) has been proven to be a promising imaging technique due to its ability to provide high resolution images at enhanced contrast related to the optical absorption [1,2]. In addition, PAI does not cause harmful effects to the patient. Photoacoustic (PA) waves are generated from a tissue when it is subjected to a pulsed laser irradiation. The energy carried by each laser pulse causes a local increase of temperature of the tissue, related to its optical absorption, leading to a thermal expansion, which generate an acoustic perturbation in the ultrasound frequency range [3,4]. The resulting ultrasound (US) waves propagate through the tissue to the body surface where they can be detected [4].

The advantages of PAI rely on its hybrid nature and the combination of the two imaging methods: optical imaging and ultrasound imaging. By coupling them, this modality overcomes some of their limitations. More precisely, PAI features resolution of ultrasound imaging while its contrast derives from the optical absorption. This imaging modality is particularly interesting for vascular imaging as blood is a strong optical absorber in the near infrared and presents a good contrast with the surrounding medium [5].

The theoretical PA signal generated by a spherical absorber surrounded by a lossless medium is a short pulse, characterized by a single-cycle shape, which is often referred to as N-shaped. This

* Corresponding author.
E-mail address: francois.varray@creatis.insa-lyon.fr (F. Varray).

http://dx.doi.org/10.1016/j.pacs.2017.09.001

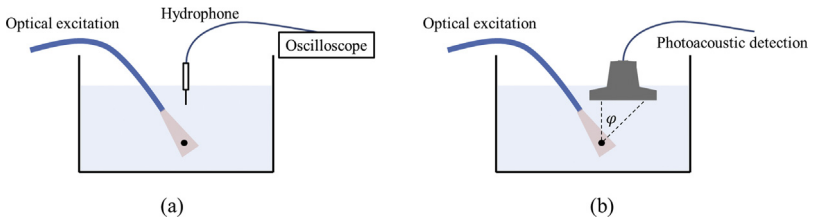

Fig. 1. Experimental set-up for the pure receive impulse response of the US probes of the study. The computation is made in two steps: (a) receiving the signal on the hydrophone, (b) receiving the same signal on the US probes. The φ angle allows evaluating the acceptance angle of the various probes.

shape results from the summation of a diverging compressive wave coming from the absorber and a converging compressive wave coming from the center of the absorber and reaching the detector with a delay, as a rarefaction wave [6]. The frequency bandwidth of a PA signal increases as the absorber gets smaller. Consequently, the spectral content of a PA signal generated by biological tissues may range from 1 MHz up to 100 MHz [4,6].

PA signals can be recorded using an US probe coupled with an US scanner. However, classical piezoelectric US probes, using PZT technology, have a limited bandwidth in both transmission and reception. An emerging alternative technology, CMUT (capacitive micromachined ultrasound transducer, [7]), can overcome this limitation. As compared to conventional PZT transducers, CMUTs may offer higher sensitivity and wider bandwidth [8]. As specifically regards reception (RX) operation in ideal electrical loading conditions, while the voltage frequency response of PZT transducers has a band-pass characteristic, CMUTs exhibit low-pass voltage [9] and charge [10] RX frequency responses theoretically reaching a 200% fractional bandwidth in reception. Such peculiar broadband characteristic, together with the higher RX sensitivity, motivated the first investigations on the use of CMUTs in PAI [11,12]. Several research groups have researched on the potential of CMUTs for PAI. In [13], *in vitro* three-dimensional PAI results using 2D CMUT arrays were successfully obtained. In [14], a particular CMUT technology was established to fabricate an optical-acoustic integrated PA imager, consisting of an infrared-transparent US array backed by an optical source. Furthermore, the technological advantages of CMUTs were exploited in the realization of miniaturized arrays for both two-dimensional [15] and three-dimensional [16] endoscopic PAI. However, the current literature lacks information on the potential performance increase achievable by using CMUT technology in place of classical PZT technology. Only recently, a RX-mode operation performance comparison between a PZT linear probe and an equivalent CMUT probe was carried out [17,18], and the benefits achievable by the higher sensitivity and the wider acceptance angle of the CMUT probe were discussed in a PA imaging application context.

This paper explores the potential advantages achievable by using CMUT technology for PA applications through a qualitative and quantitative imaging assessment. A preliminary study was conducted in [19] and is extended hereafter. A comparative study is carried out by conducting *in vitro* imaging experiments on a suture wire and on bimodal phantoms using different PZT and CMUT probes. Two CMUT linear probes, developed and manufactured by different research laboratories, were used in conjunction with open US scanners to acquire PA signals and generate PA images of the phantoms. The same experiments were carried out using two linear PZT commercial probes from different manufacturers. Qualitative and quantitative criteria, based on the computation of pure receive impulse response, signal-to-noise ratio (SNR) and contrast-to-noise ratio (CNR), were used to assess PA image quality.

2. Materials

2.1. Photoacoustic experimental set-up

The PA imaging set-up employed for this study consists of a Q-switched Nd:YAG laser at 1064 nm (Quanta-ray INDI, Spectra-Physics) delivering 5-ns laser pulses at a repetition rate of 10 Hz. The beam diameter is 8 mm. The spatial impulse response was measured using a 100 μm black absorbing suture wire (Ethilon 5-0, Polyamid 6, Ethicon) placed in a water tank. The suture wire was illuminated through the Nd:Yag source coupled with a 10-mm fiber bundle (CeramOptec GmbH, Bonn, Germany) composed of 431 individual optical fibers, each with 0.3 mm silica core diameter and 0.22 numerical aperture. In all measurements, the illumination position was fixed with respect to the suture wire position. The photoacoustic signal detection was made first with a needle hydrophone (Preamplifier W235052, Precision Acoustics), vertically placed 25 mm above the suture wire, using an oscilloscope. The frequency band of the hydrophone is wide enough in order to acquire the complete spectral content of the PA signal generated by the suture wire. The measured signal is averaged over 100 acquisitions. Then, the detection of the same PA signal is conducted using the different US probes used in this study. In all measurements, the probes were positioned in a way that the distance between the suture wire and the closest probe element, i.e. the border element of the active aperture, is set to the same distance of 25 mm. The PA signal was then acquired using all the elements of the active aperture in order to evaluate the angular acceptance of the probes, i.e. the evolution of the reception frequency response as a function of the arrival angle of the PA signal on the probe. The experimental setup is highlighted in Fig. 1.

For the phantom acquisitions, the laser beam was directed towards the phantoms while the US probe was positioned perpendicularly to the laser excitation, as shown in Fig. 2. The signal reception was optimized by improving the US coupling between the probe and the phantom using US gel. The described set-up allows recording simultaneously both PA and US images.

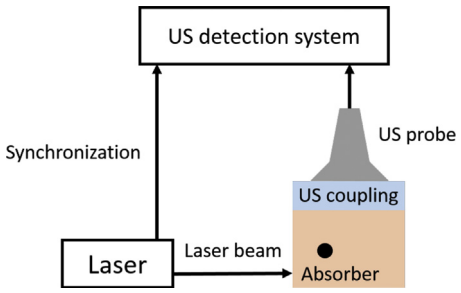

Fig. 2. Experimental photoacoustic set-up. An optical pulse illuminates the medium and the absorbers. A photoacoustic signal is generated and received by the US probe and post-processed by the scanner.

Table 1
Characteristics of the US probe used in the experiments in conjunction with the SonixMDP and the ULA-OP system. The values are given by the manufacturers of the probes.

	SonixMDP		ULA-OP	
	PZT L14-5W/60	CMUT Vermon	PZT LA523E	CMUT ACULAB
Central frequency (MHz)	7.5	8.9	8.5	10
−6 dB fractional bandwidth (pulse-echo measurement)	80%	70%	92%	100%
Number of elements	128	128	192	192
Pitch (μm)	472	150	245	200

2.2. Ultrasound imaging experimental set-up

In order to compare CMUT and PZT transducer technologies, four different linear probes with rather similar characteristics were employed in the experiments. The two CMUT probes are a 128-element, 8.9 MHz linear probe from Vermon (Vermon SA, Tours, France), and a 192-element, 10 MHz linear probe from ACULAB (Department of Engineering, Roma Tre University, Rome, Italy). The two commercial PZT probes are the L14-5W/60 128-element, 7.5 MHz linear probe (Prosonic Co., Gyeongsangbuk-do, Korea) and the LA523E 192-element, 8.5 MHz linear probe (Esaote S.p.A., Florence, Italy).

Being provided with different system connectors, the four probes could not be used on the same US scanner. Therefore, two different US scanners have been used in this study. The first one is the clinical US scanner SonixMDP (Ultrasonix, Analogic Corp, Peabody, MA, USA), coupled with the additional SonixDAQ acquisition module. This module allows the acquisition of raw radiofrequency (RF) prebeamforming data on 128 independent RX channels, and the synchronisation of the US scanner and the laser system. The second US scanner is the Ultrasound Advanced Open Platform (ULA-OP, MSDLab, University of Florence, Florence, Italy), which can be fully programmed and allows controlling up to 64 independent RX channels [20].

The basic characteristics of the probes and the corresponding US system employed are summarized in Table 1.

2.3. Phantoms

Bimodal phantoms, constituted of optical absorbers embedded in tissue mimicking materials, have been specifically manufactured for this experimental study. Two components have been selected for the bulk material: PVA cryogel (PolyVinyl Alcohol, 10%) and agar (Agar agar 4%). These two materials exhibit a different reduced scattering coefficient. A high reduced scattering coefficient implies that only a small fraction of the incoming laser light will reach the absorber, leading to a low PA signal to be detected by the US probe. After 5 freeze cycles, the PVA cryogel presents a reduced scattering coefficient of about $\mu_s' = 4\,\mathrm{cm}^{-1}$ [21], along with a negligible absorption coefficient ($\mu_a \ll 1\,\mathrm{cm}^{-1}$) and a speed of sound of 1520 m s^{-1}. The reduced scattering coefficient in agar is about $\mu_s' = 1\,\mathrm{cm}^{-1}$, the absorption coefficient is negligible and the speed of sound is about 1475 m s^{-1}. For each material, a spherical inclusion (10 mm in diameter) of the bulk material is included. The inclusion was previously coloured by India ink (concentration of 0.03%). They are approximatively 1 cm deep from the external surface. Pictures of the phantoms used for this comparative study are presented Fig. 3. In Fig. 3(c), a picture of the tainted inclusion before being embedded in the phantom is also provided.

3. Methods

3.1. Calibration of the SonixMDP and the ULA-OP

To obtain comparable values and signals on the SonixMDP and the ULA-OP systems, a calibration procedure has been established. A custom-built adaptor was designed and fabricated in order to connect the PZT L14-5W/60 and the CMUT Vermon probes, which are both provided with the SonixMDP system connector, to the ULA-OP, allowing the raw RF signals acquisition. However, because the ULA-OP hardware allows simultaneous acquisition of only 64 signals, the acquisitions were conducted in two steps in order to collect the signals of the entire arrays. An agar phantom with a strong tainted inclusion was illuminated with the laser. For each probe and for a given driving laser amplitude, the received echoes were stored on both the SonixMDP and the ULA-OP systems. For each reconstructed image, the maximum amplitude inside the inclusion was extracted. The ratio between the two values gave the conversion ratio between the SonixMDP and the ULA-OP for the same laser excitation, corresponding to the same initial photoacoustic signal. By changing the excitation amplitude of laser, the conversion ratio evolution between the SonixMDP and the ULA-OP was computed.

3.2. Evaluation of the receive impulse response

Using the proposed experimental setup proposed in Fig. 1, the pure receive impulse response of the transducer can be computed from the signals detected by the hydrophone and the probe element. Indeed, the signal received by the probe element, $s(t)$, can be expressed as

$$s(t) = IR_{RX}(t) * s_{PA}(t) \quad (1)$$

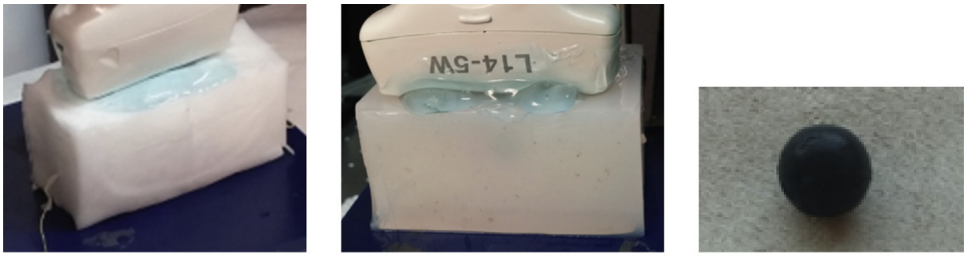

Fig. 3. Pictures of the bimodal phantoms used for this study (a) PVA blocks (10% – 5 cycles) and (b) agar. Each one contains an inclusion of the same material (c) coloured with India ink (concentration of 0.03%).

where $IR_{RX}(t)$ is the pure receive impulse response of the probe element and s_{PA} is the PA signal generated by the suture wire and detected by the hydrophone. The IR_{RX} can be conveniently computed in the frequency domain as [10]:

$$\log_{10}(IR_{RX}(f)) = \log_{10}(S(f)) - \log_{10}(S_{PA}(f)) \quad (2)$$

The −6 dB center frequency in reception and bandwidth are computed from the resulting spectrum by finding the two −6 dB cutoff frequencies f_{high} and f_{low}. Then, the fractional bandwidth is computed as percentage ratio between the −6 dB bandwidth and center frequency as

$$BW_{-6dB} = 2\frac{f_{high} - f_{low}}{f_{high} + f_{low}} \cdot 100\% \quad (3)$$

To evaluate the acceptance angle of each probe, the spectra of the signals received by all the probe aperture elements are evaluated as a function of the angle φ, following the measurement procedure proposed in [18]. The subtraction of the hydrophone signal is also conducted to evaluate only the receive IR of each probe element. For each probe, the spectral sensitivity is evaluated in the [0°; 35°] range.

3.3. Phantom acquisitions

Three comparative studies have been carried out. The first two studies compare two pairs of probes (PZT and CMUT) connected to two different US scanners using the same targeted agar medium with the coloured inclusion. The third study compares the ULA-OP PZT and CMUT probes on the PVA tissue mimicking materials, which present a higher optical scattering coefficient. The acquisitions strategy is summarised in Table 2.

The three studies are made with both US probes at several energy levels up to 195 mJ/pulse. For each configuration, a background image has been taken, without any laser excitation, to evaluate the global noise of the system. For each energy level, thirty frames with the full array on a few centimetres depth are saved before proceeding to the image reconstruction. For each phantom, an ultrasonic image (B mode image) has also been recorded in the same configuration. Hence the PA signals can be overlaid on the corresponding B-mode image.

3.4. Image reconstruction

The acquired data are reconstructed using k-Wave package [22]. The echoes initially received by the linear probes are expressed in the Fourier domain and then resampled to beamform the image. The used sampling in the Fourier domain is defined by:

$$\begin{cases} k_t \in [0; \pi/dt] \\ k_x \in [0; c\pi/dx] \\ k = \sqrt{k_t^2 + k_x^2} \end{cases} \quad (4)$$

where dt being the sampling time, dx being the lateral spatial sampling, c is the speed of sound, k_t and k_x are the temporal and spatial wave numbers. The focalisation of received echoes is processed by re-sampling the spectra. Hence, for each spatial line of the spectra, an interpolation is made from the k_t axis on the modified k axis. This way, the echoes are focused and a better reconstruction from PA signals as compared to the delay-and-sum algorithm is obtained [22]. Another advantage is its calculation speed and its real-time implementation.

Table 2
Acquisition strategy. In study 1 and 2, the same Agar phantom is scanned using the two US scanners with the four probes. In study 3, the PVA phantom is scanned using the ULA-OP and the corresponding probes.

Study	Probes			US scanner	Phantom
1	PZT L14-5W/60	–	CMUT Vermon	SonixMDP	Agar
2	PZT LA523E	–	CMUT ACULAB	ULA-OP	Agar
3	PZT LA523E	–	CMUT ACULAB	ULA-OP	PVA

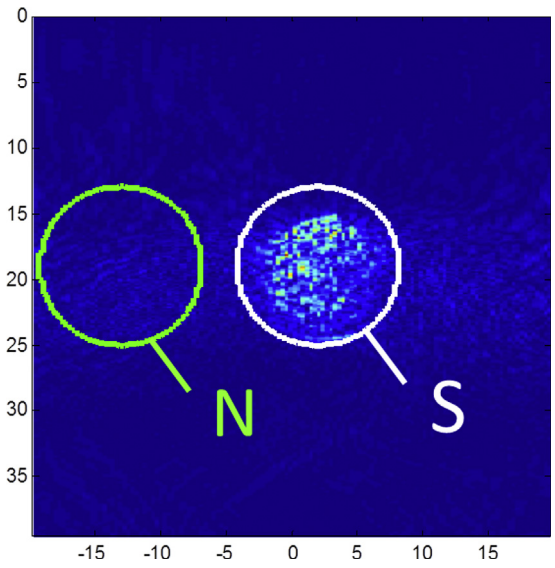

Fig. 4. Example of noise (N) and signal (S) ROI.

3.5. Quantification

Two criteria have been used to evaluate the images quality and compare the acquisitions made with PZT and CMUT probes: the signal-to-noise ratio (SNR) and the contrast-to-noise ratio (CNR). To calculate such indexes, two regions of interest (ROI) were defined on the images of the spherical inclusions: one for the signal (S) and one for the noise (N). These ROI are circles of 10 mm in diameter. Fig. 4 shows an example of two ROI.

The SNR and CNR are calculated from the following expressions [23]:

$$\mathrm{SNR} = 20 \log_{10}\left(\frac{\overline{S}}{\overline{N}}\right) \quad (5)$$

$$\mathrm{CNR} = 20 \log_{10}\left(\frac{\left|\left|\overline{S} - \overline{N}\right|\right|}{\sigma_0}\right) \quad (6)$$

$\overline{(.)}$ being the mean in the defined ROI and σ_0 being the standard deviation of pure noise in the ROI.

4. Results

4.1. SonixMDP and ULA-OP calibration

For the calibration, 5 different energy levels were used on the laser. The used energy levels are 125, 160, 175, 190 and 195 mJ/impulsion. For each acquisition on the ULA-OP or the SonixMDP, the mean and standard deviation of the received amplitude were computed. The resulting curve is presented in Fig. 5. A linear regression was computed with an R^2 value of 98.5%. For each new SonixMDP acquisition, this calibration allowed converting the acquired PA signals into the ULA-OP range, making it possible to compare acquisitions carried out with different scanners.

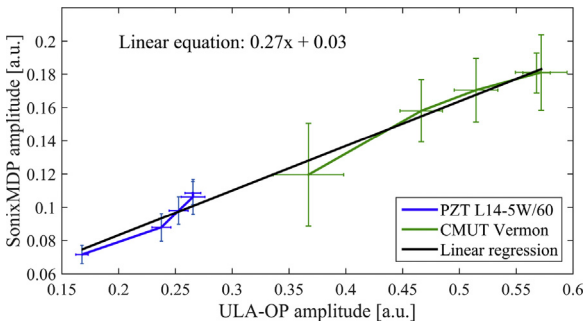

Fig. 5. Calibration curve of the SonixMDP and ULA-OP system using the same probes.

However, given the limited numbers of active elements of the ULA-OP, the acquisitions of study 1 are still conducted with the SonixMDP in order to directly acquire the PA signal on the whole array for its native probes (PZT L14-5W/60 and CMUT Vermon).

4.2. Receive impulse response measurement

For each acquisition on the ULA-OP system, an accumulation of 100 acquisitions has been conducted. Fig. 6 depicts the obtained frequency responses in pure reception, and Table 3 reports the corresponding center frequencies, the −6 dB cutoff frequencies, the fractional bandwidths and the peak sensitivities. It can be noticed that the reception frequency response of both CMUT probes is centered at a lower frequency, and is characterized by a significantly larger fractional bandwidth as compared to the PZT probes. In terms of peak sensitivity, the values reported in Table 3 are referred to the highest value that was achieved with the CMUT ACULAB probe.

In Fig. 7, the spectral sensitivity of the four probes as a function of the incident angle is proposed. A quantitative comparison between the results is not straightforward since the four probes have different element widths resulting in different element directivity, being the acceptance angle partially related to these parameters. Qualitatively, the spectral sensitivity of the two CMUT probes shows a lower variation as a function of the angle as compared to the PZT ones. In the particular case of the CMUT ACULAB and the LA523E PZT probes, the results can be more fairly compared. Indeed, the CMUT ACULAB array has a 200 μm pitch with a practically zero kerf, and the LA523E PZT probe has a 245 μm pitch with a 30 μm kerf, leading to a 215 μm element width. The similarity between the two element widths allows a fair comparison between the spectral sensitivities. As can be observed, the sensitivity reduction as a function of the incident angle, in the frequency range 3.2–7.1 MHz, where the reception −6 dB bands of the two probes overlap, is lower for the CMUT probe, evidencing its broader acceptance angle.

4.3. Comparison of the PZT and CMUT probes on the agar phantom

The studies 1 and 2 compare the two probe technologies on the same phantom. This comparison is conducted on two different scanners: one pair of PZT/CMUT probes is used on each system (Table 2).

Fig. 8 shows PA images obtained on the agar phantoms containing the coloured spherical inclusions with the different tested probes. On this phantom, the SNR and CNR have been calculated for the different values of the excitation energy and for both probes of each pair. Results are shown in Fig. 9.

This comparative study shows a significant improvement of the SNR and CNR when using the CMUT technology for each probes pair. The SNR is increased by up to 14 dB and the CNR up to 20 dB. Nonetheless, it can be observed that the results obtained by the

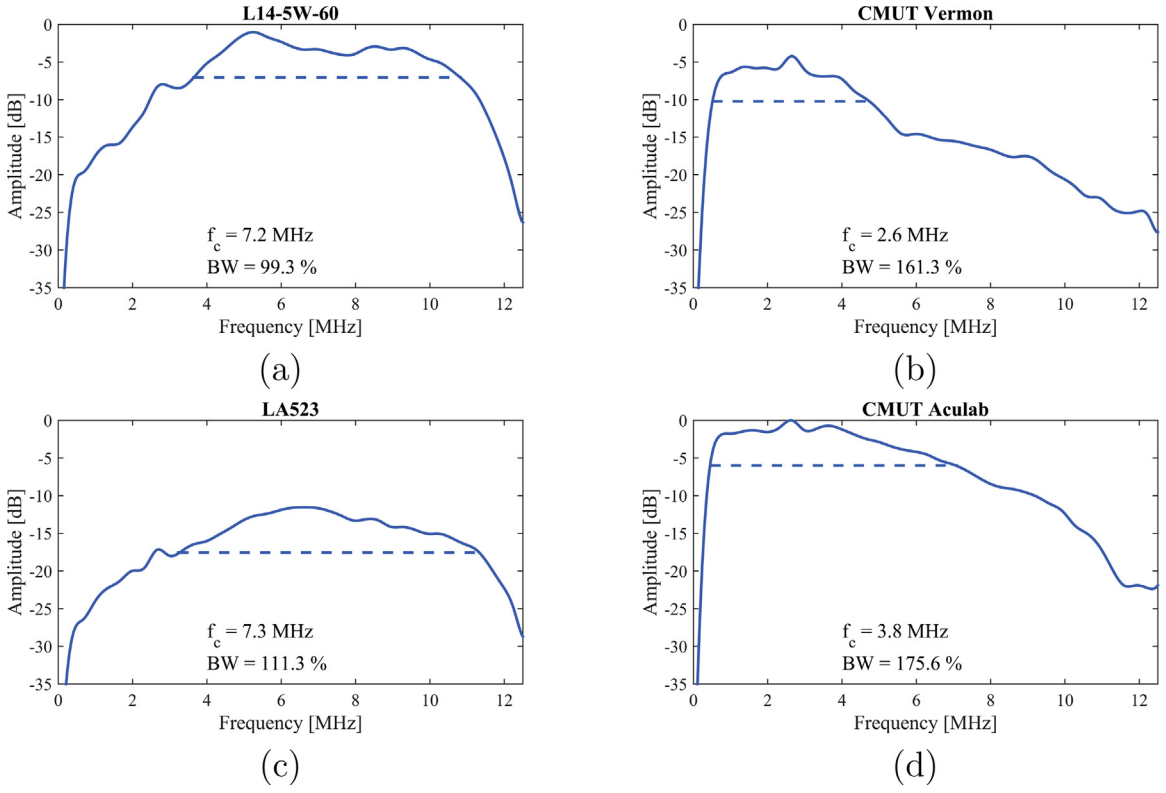

Fig. 6. Pure reception frequency response of the four probes. For each probe, the −6 dB central frequency and bandwidth are reported.

Table 3
Reception frequency response performance comparison.

	PZT L14-5W/60	CMUT Vermon	PZT LA523E	CMUT ACULAB
Central frequency (MHz)	7.2	2.6	7.3	3.8
−6 dB frequency interval (MHz)	[3.6; 10.8]	[0.5; 4.8]	[3.2; 11.3]	[0.5; 7.1]
Bandwidth	99.3%	161.3%	111.3%	175.6%
Peak sensitivity (dB)	−1.0	−4.2	−11.6	0

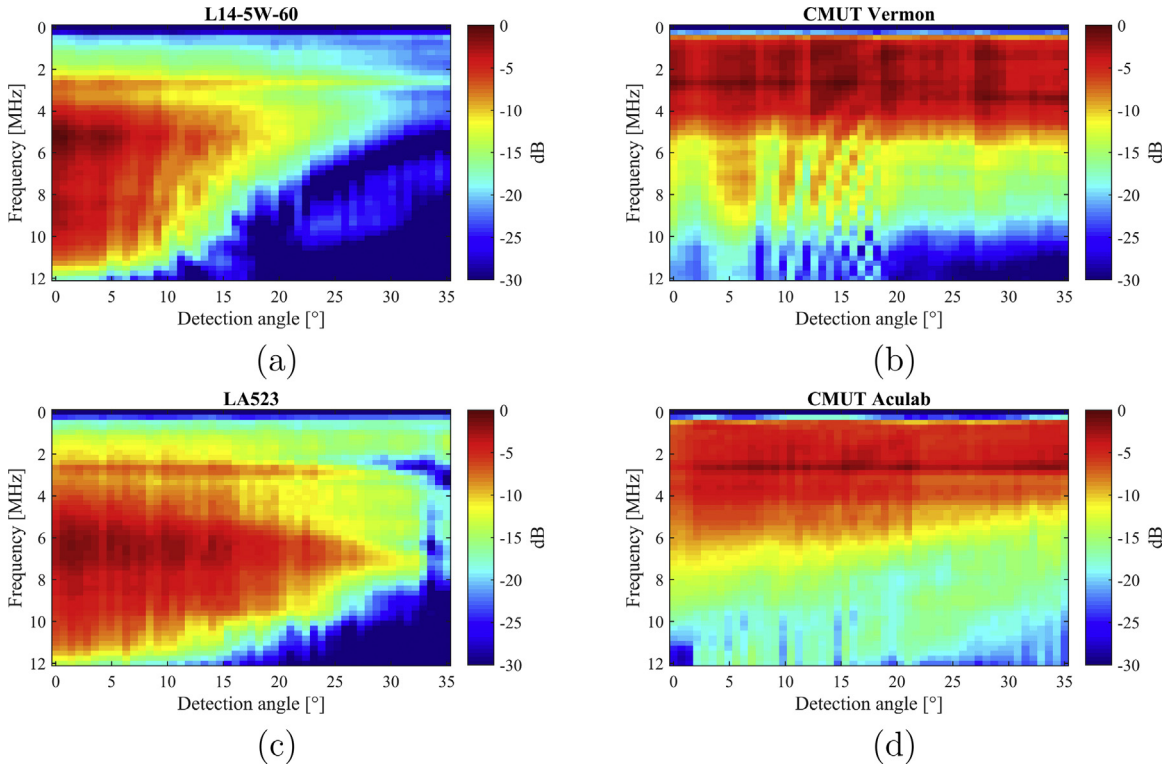

Fig. 7. Spectral sensitivity of the four probes measured as a function of the incident angle.

LA523E PZT probe and Vermon CMUT probe are similar and that the LA523E has even a better CNR that the Vermon CMUT probe.

4.4. Enhancement of the PA image quality on a highly scattering phantom

The previous comparison has highlighted the interest of the CMUT technology for PA imaging. It enhances the image quality even at a relatively low input energy, which also means a low PA signal reaching the probe. This is crucial in clinical conditions when the medium complexity and high scattering coefficient prevents most of the input photons to reach the absorber.

With this in mind, the CMUT probe giving the best results, i.e. CMUT ACULAB, has been tested on a more scattering phantom made of PVA. The results are then compared with the ones from the PZT probe of the same pair, on both agar and PVA phantoms. The corresponding reconstructed images are displayed in Fig. 10. Fig. 11 presents the calculated SNR and CNR for both probes and on both phantoms for different values of the excitation energy.

From Fig. 10, it can be observed that, where the PZT probe fails to detect enough signal to reconstruct the inclusion image, the CMUT probe detects more signal coming from the inclusion, giving more information about the imaged medium. The SNR values in the PVA phantom are higher with the CMUT ACULAB, from a few dB up to 20 dB (Fig. 11).

5. Discussion

The imaging performance of CMUT and PZT probes was quantitatively assessed and compared in a PA experimental set up. *In vitro* images of custom designed bimodal phantoms were achieved using four different CMUT and PZT probes and two US scanners. By using the proposed calibration procedure, the data acquired with the two different scanners were made comparable. The characterization in pure reception showed that the CMUT probes, which are both provided with high-input-impedance voltage buffers integrated in the probe handle, exhibit a low-pass frequency response, resulting in an increased sensitivity at lower frequencies and a greater fractional bandwidth as compared to the PZT probes. Moreover, the CMUT ACULAB probe showed an increased peak sensitivity as compared to the CMUT Vermon probe. The spectral sensitivity measurements as a function of the incident angle generally showed that, with the CMUT probes, the frequency content is better preserved as a function of the angle between the PA signal source and the probe element as compared to the PZT probes. The performance of the CMUT Vermon is slightly better than the CMUT ACULAB due to the smaller pitch and element width (150 μm vs. 200 μm). For the phantoms acquisitions, in order to ensure repeatability of measurements, particular attention was devoted, during phantoms design and fabrication, on the dimensioning and positioning of the inclusions in the

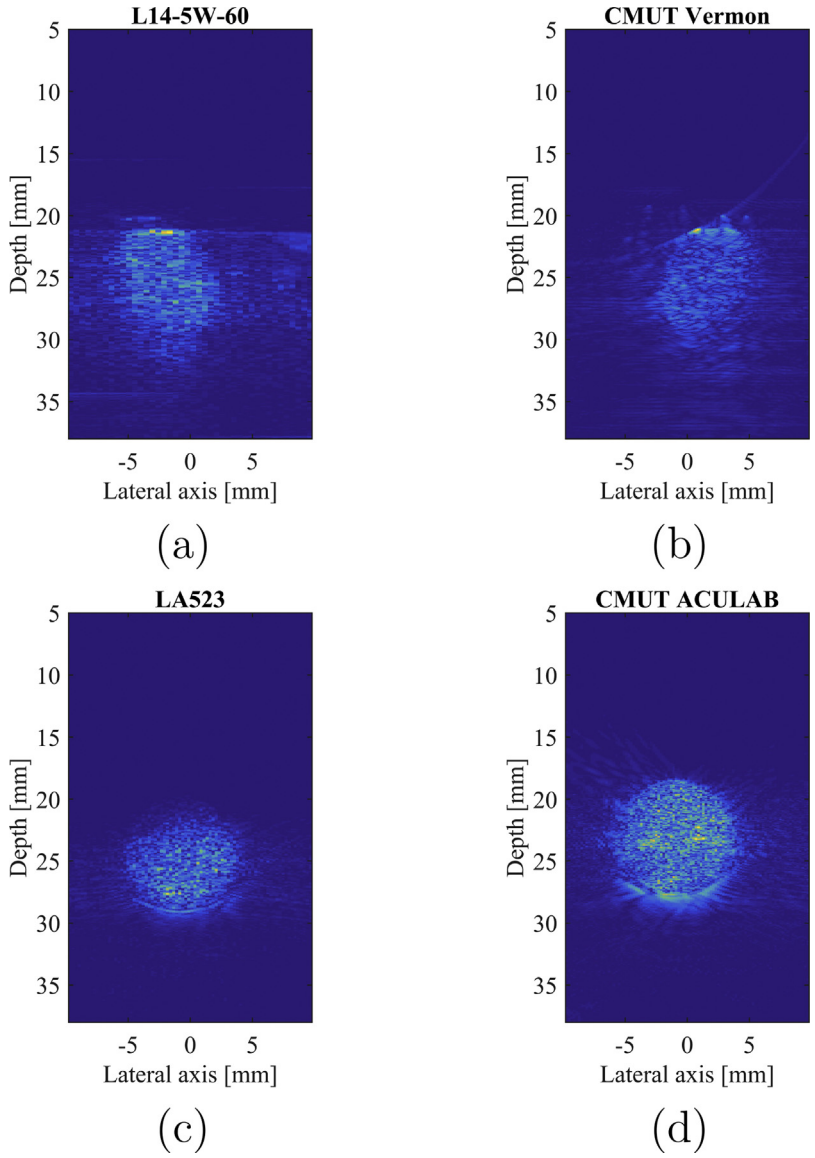

Fig. 8. PA images of the spherical inclusion made of coloured agar obtained with both probes of the two following pairs at 195 mJ/pulse: (a) L14-5W/60 (PZT) and (b) CMUT Vermon, and (c) LA523E (PZT) and (d) CMUT ACULAB.

surrounding medium. The experimental imaging results obtained in the experiments showed that, in general, a qualitative and quantitative improvement was achieved using the CMUT probes. In fact, on each scanner, the SNR and CNR computed on the images reconstructed from the data acquired with the CMUT probe were higher. In the PVA phantom experiments, in particular, the detection and correct reconstruction of the coloured inclusion was possible only using the CMUT probe.

The proposed study suffers from some limitations. First, to compare the signals received on the four probes, a calibration step has been conducted in a photoacoustic experiment. Based on a custom-built adaptor, it allows to acquired on a single US scanner the PA signals received on all probes. For the comparison between two probes, the acquisitions have been conducted on the same phantom. The position was not changed during the experiment and the laser excitation was set at the same location. However, note that for the comparison study we chose to keep connected the probes to their native scanners in order to get the benefits of the settings parameters adapted to each scanner. Of course, the position of the probe on the phantom may have slightly changed between two acquisitions but this change is limited and the alignment of the probe has been carefully optimized for each situation. However, the SNR and CNR comparison did not allow directly concluding that CMUT probes are better than PZT. Indeed, based on these two criteria, the performance of the LA523E and CMUT Vermon probes are close. Last, the four used probes are different in terms of pitch and or number of active elements. However, the observed maximal PA amplitudes detected in the whole images are in accordance with the obtained SNR and CNR trends. The study of PZT and CMUT probes having the same geometrical design may be the optimal solution to evaluate both probe performances. However, such hardware solution is not currently available.

In the proposed comparison, the noise equivalent pressure (NEP) of our arrays has not been conducted. Indeed, we the variability of the used probes and systems, such measurement will surely by very sensitive to other parameters that cannot be practically controlled during the acquisition. Similarly, values of the NEP can be found in the literature for CMUT arrays, $\sim$2 mPA/$\sqrt{\text{Hz}}$ [13,24] and PZT probe [0.2; 0.6] mPA/$\sqrt{\text{Hz}}$ [25]. Moreover, the

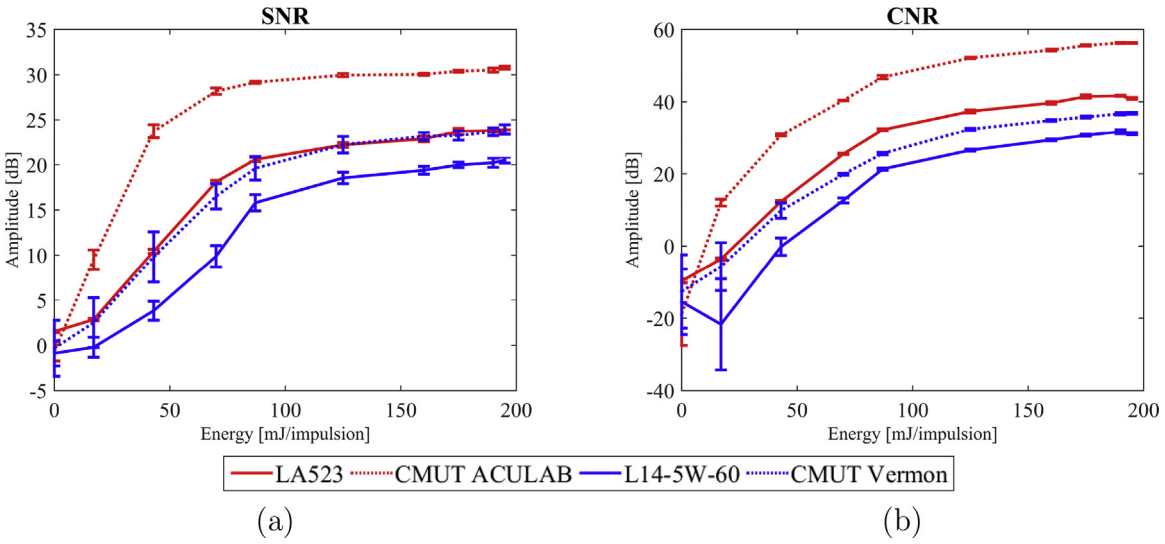

Fig. 9. Evolutions of the SNR and CNR as a function of the excitation energy for both probes types of each pair in the agar phantom (study 1 and 2, Table 2).

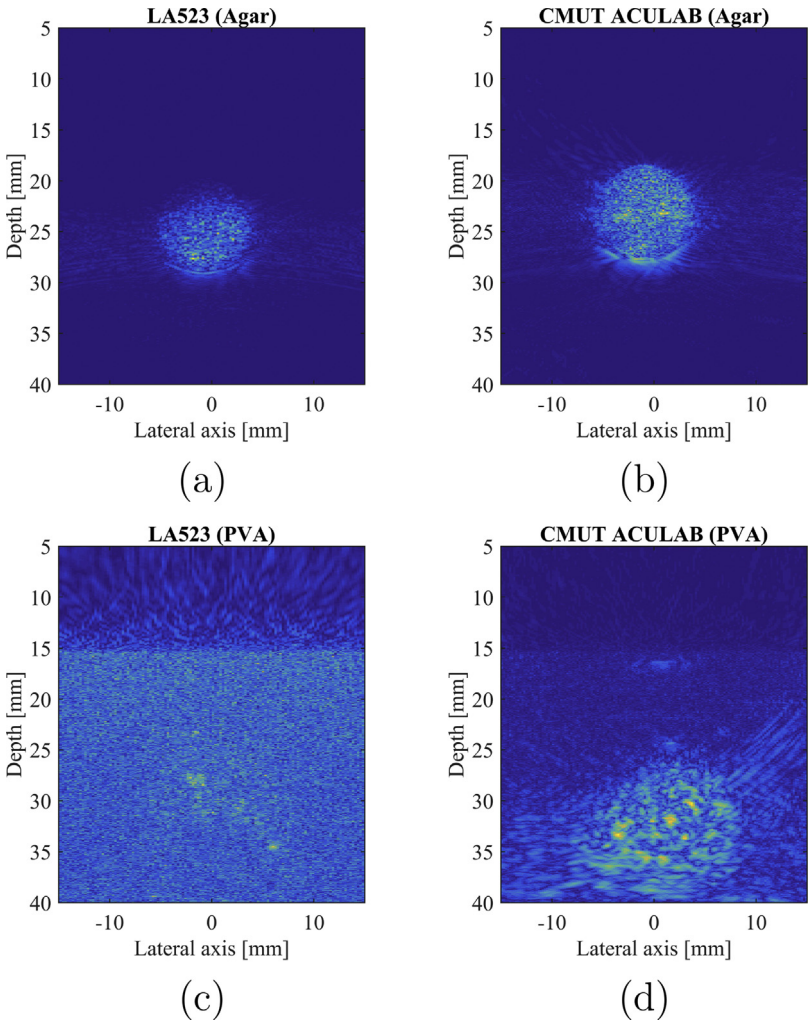

Fig. 10. PA images of the spherical inclusion made of coloured (a, b) Agar and (c, d) PVA obtained with both probes of the same pair at 195 mJ/pulse: (a, c) LA523E (PZT) and (b, d) CMUT ACULAB.

resolution may appear as a good criterion to evaluate the performance of the various probes. Indeed, in our study, the number of element and their pitch are different on each probe and such parameters are highly related to the lateral resolution. Moreover, the axial resolution is related to the absolute frequency bands, which are also quite different among the probes. The

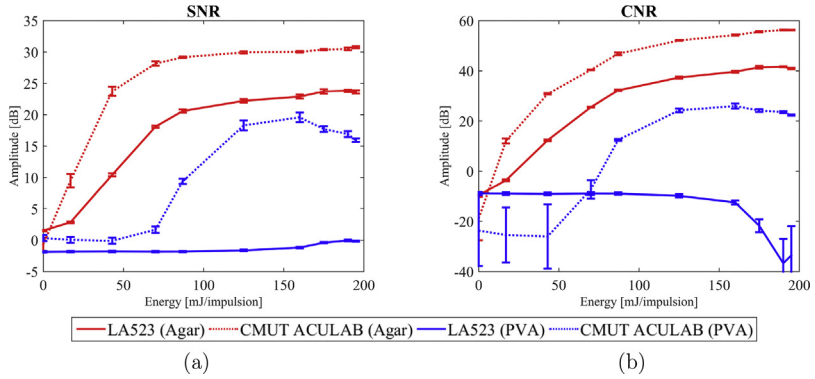

Fig. 11. Evolutions of the SNR and CNR as a function of the excitation energy for the PZT and CMUT probes of the same pair on both the agar and the PVA phantoms (study 2 and 3, Table 2).

obtained resolution will then be difficult to compare between them.

The application of CMUT technology to PAI is advantageous for many reasons. As it was proven in this paper, the larger RX bandwidth allows dramatically improving the detection sensitivity, leading to an increased quality of PA images. As concerns medical imaging applications, a higher sensitivity may be a highly appreciated property of a transducer used in PA clinical conditions since it allows both reducing the optical excitation energy and improving the penetration depth. Moreover, other CMUT characteristics, mainly related to the fabrication technology, may be leveraged in PA applications. The possibility of fabricating transducer arrays with particular shapes, such as sparse or ring arrays, together with the opportunity of making the device transparent to light propagation, opens a big opportunity in the fabrication of high-performance miniaturized PA integrated imagers. Besides the first investigations reported in [14], where infrared transparency was achieved by thinning the silicon microfabrication substrate down to 100 μm, the successful microfabrication of CMUTs on an optically transparent substrate (i.e. glass), was shown in [26,27]. Furthermore, CMUT with through-glass-via interconnects fabrication was reported in [28], possibly enabling the access to 3D-integration technologies. Finally, Reverse Fabrication Process [29], i.e. the CMUT technology used for the fabrication of the CMUT ACULAB probe tested in this paper, allows the application of a custom backing directly to the CMUT array [30], after the microfabrication on standard silicon substrates. Current research is devoted to the study of novel CMUT probes for three-dimensional PAI applications, based on the use of particular 2D array configurations, and both acoustically and optically optimized packaging materials.

6. Conclusion

The proposed study confirmed that the higher acceptance angle obtainable with CMUTs represents one of the advantages of using such transducer technology in PAI applications. In addition to previous studies, it demonstrated that the CMUT higher sensitivity and wider reception fractional bandwidth represents another important characteristic for detecting signals where the spectral content is distributed over a very wide frequency range, such as in PAI. Even though the four probes used have different characteristics in terms of array geometry and frequency response, the experimental results support the conclusions, suggesting that the potential of CMUT technology can be further leveraged in PAI applications by optimizing the design for high reception sensitivity and wideband operation.

Conflict of interest

The authors declare no conflicts of interest.

Acknowledgments

This work was supported by the LABEX CELYA (ANR-10-LABX-0060) and PRIMES (ANR-11-LABX-0063) of Universitéé de Lyon, within the program “Investissements d’Avenir” (ANR-11-IDEX-0007) operated by the French National Research Agency (ANR). The CMUT probe from Vermon was part of the program ANR BBMUT of Université de Lyon. The CMUT probe from ACULAB was part of the collaborative research agreement between the Department of Engineering of Roma Tre University and CREATIS, University of Lyon. This work was also partially supported by ITN-FP7 OILTEBIA.

References

[1] J.L. Su, B. Wang, K.E. Wilson, C.L. Bayer, Y.-S. Chen, S. Kim, K.A. Homan, S.Y. Emelianov, Advances in clinical and biomedical applications of photoacoustic imaging, Expert Opin. Med. Diagn. 4 (6) (2010) 497–510.
[2] D.R. Bauer, R. Olafsson, L.G. Montilla, R.S. Witte, 3-d photoacoustic and pulse echo imaging of prostate tumor progression in the mouse window chamber, J. Biomed. Opt. 16 (2) (2011) 026012.
[3] A.G. Bell, Upon the production and reproduction of sound by light, J. Soci. Telegr. Eng. 9 (34) (1880) 404–426.
[4] C. Li, L. Wang, Photoacoustic tomography and sensing in biomedicine, Phys. Med. Biol. 54 (19) (2009) 59–97.
[5] X.L. Deán-Ben, D. Razansky, Functional optoacoustic human angiography with handheld video rate three dimensional scanner, Photoacoustics 1 (3–4) (2013) 68–73.
[6] G.J. Diebold, T. Sun, M.I. Khan, Photoacoustic monopole radiation in one, two, and three dimensions, Phys. Rev. Lett. 67 (24) (1991) 3384–3387.
[7] A. Ergun, Y. Huang, X. Zhuang, O. Oralkan, G. Yaraholu, B. Khuri-Yakub, Capacitive micromachined ultrasonic transducers: fabrication technology, IEEE Trans. Ultrason. Ferroelectr. Freq. Control 55 (2) (2008) 327–342.
[8] A. Savoia, G. Caliano, B. Mauti, M. Pappalardo, Performance optimization of a high frequency CMUT probe for medical imaging, IEEE International Ultrasonics Symposium, (2011) , pp. 600–603.
[9] X. Jin, O. Oralkan, F.L. Degertekin, B.T. Khuri-Yakub, Characterization of one-dimensional capacitive micromachined ultrasonic immersion transducer arrays, IEEE Trans. Ultrason. Ferroelectr. Freq. Control 48 (3) (2001) 750–760.
[10] A.S. Savoia, G. Caliano, A. Mazzanti, M. Sautto, A.D. Leone, D.U. Ghisu, F. Quaglia, An ultra-low-power fully integrated ultrasound imaging CMUT transceiver featuring a high-voltage unipolar pulser and a low-noise charge amplifier, IEEE International Ultrasonics Symposium, (2014) , pp. 2568–2571.
[11] I.O. Wygant, D.T. Yeh, X. Zhuang, S. Vaithilingam, A. Nikoozadeh, O. Oralkan, A. Sanli Ergun, G.G. Yaralioglu, B.T. Khuri-Yakub, Integrated ultrasound imaging systems based on capacitive micromachined ultrasonic transducer arrays, IEEE Sensors, (2005) , pp. 704–707.
[12] S. Vaithilingam, I.O. Wygant, P.S. Kuo, X. Zhuang, O. Oralkan, P.D. Olcott, B.T. Khuri-Yakub, Capacitive micromachined ultrasonic transducers (CMUTS) for photoacoustic imaging, Proc. SPIE, Photons Plus Ultrasound: Imaging and Sensing, vol. 6086, (2006) , pp. 608603.
[13] S. Vaithilingam, T.J. Ma, Y. Furukawa, I.O. Wygant, X. Zhuang, A.D.L. Zerda, O. Oralkan, A. Kamaya, S.s. Gambhir, R.B. Jeffrey, B.T. Khuri-yakub, Three-

dimensional photoacoustic imaging using a two-dimensional CMUT array, IEEE Trans. Ultrason. Ferroelectr. Freq. Control 56 (11) (2009) 2411–2419.
[14] J. Chen, M. Wang, J.C. Cheng, Y.H. Wang, P.C. Li, X. Cheng, A photoacoustic imager with light illumination through an infrared-transparent silicon CMUT array, IEEE Trans. Ultrason. Ferroelectr. Freq. Control 59 (4) (2012) 766–775.
[15] A. Nikoozadeh, J.W. Choe, S.R. Kothapalli, A. Moini, S.S. Sanjani, A. Kamaya, Oralkan, S.S. Gambhir, P.T. Khuri-Yakub, Photoacoustic imaging using a 9F microlinear CMUT ice catheter, 2012 IEEE International Ultrasonics Symposium, (2012) , pp. 24–27.
[16] A. Nikoozadeh, C. Chang, J.W. Choe, A. Bhuyan, B.C. Lee, A. Moini, P.T. Khuri-Yakub, An integrated ring CMUT array for endoscopic ultrasound and photoacoustic imaging, 2013 IEEE International Ultrasonics Symposium (IUS), (2013) , pp. 1178–1181.
[17] O. Warshavski, C. Meynier, N. Sénégond, P. Chatain, N. Felix, A. Nguyen-Dinh, Experimental evaluation of CMUT and PZT transducers in receive only mode for photoacoustic imaging, Proc. SPIE 9708, Photons Plus Ultrasound: Imaging and Sensing, (2016) 970830-7.
[18] J. Rebling, O. Warshavski, C. Meynier, D. Razansky, Optoacoustic characterization of broadband directivity patterns of capacitive micromachined ultrasonic transducers, J. Biomed. Opt. 22 (4) (2016) 041005.
[19] M. Vallet, F. Varray, M.A. Kalkhoran, D. Vray, J. Boutet, Enhancement of photoacoustic imaging quality by using CMUT technology: experimental study, IEEE International Ultrasonics Symposium, (2014) , pp. 1296–1299.
[20] E. Boni, L. Bassi, A. Dallai, F. Guidi, A. Ramalli, S. Ricci, J. Housden, P. Tortoli, A reconfigurable and programmable FPGA-based system for nonstandard ultrasound methods, IEEE Trans. Ultrason. Ferroelectr. Freq. Control 59 (7) (2012) 1378–1385.
[21] K. Zell, J.I. Sperl, M.W. Vogel, R. Niessner, C. Haisch, Acoustical properties of selected tissue phantom materials for ultrasound imaging, Phys. Med. Biol. 52 (20) (2007) N475.
[22] B.E. Treeby, B.T. Cox, k-Wave: Matlab toolbox for the simulation and reconstruction of photoacoustic wave fields, J. Biomed. Opt. 15 (2) (2010) 021314–021314-12.
[23] M. Welvaert, Y. Rosseel, On the definition of signal-to-noise ratio and contrast-to-noise ratio for FMRI data, PLOS ONE 8 (11) (2013) 1–10.
[24] I.O. Wygant, X. Zhuang, D.T. Yeh, O. Oralkan, A.S. Ergun, M. Karaman, B.T. Khuri-yakub, Integration of 2d CMUT arrays with front-end electronics for volumetric ultrasound imaging, IEEE Trans. Ultrason. Ferroelectr. Freq. Control 55 (2) (2008) 327–342.
[25] A.M. Winkler, K. Maslov, L.V. Wang, Noise-equivalent sensitivity of photoacoustics, J. Biomed. Opt. 18 (9) (2013) 097003.
[26] J. Knight, J. McLean, F.L. Degertekin, Low temperature fabrication of immersion capacitive micromachined ultrasonic transducers on silicon and dielectric substrates, IEEE Trans. Ultrason. Ferroelectr. Freq. Control 51 (10) (2004) 1324–1333.
[27] E. Bahette, J.F. Michaud, D. Certon, D. Gross, M. Perroteau, D. Alquier, Low temperature capacitive micromachined ultrasonic transducers (CMUTS) on glass substrate, J. Micromech. Microeng. 26 (11) (2016).
[28] X. Zhang, F.Y. Yamanery, Oralkan, Fabrication of capacitive micromachined ultrasonic transducers with through-glass-via interconnects, 2015 IEEE International Ultrasonics Symposium (IUS), (2015) , pp. 1–4.
[29] A. Bagolini, A.S. Savoia, A. Picciotto, M. Boscardin, P. Bellutti, N. Lamberti, G. Caliano, PECVD low stress silicon nitride analysis and optimization for the fabrication of CMUT devices, J. Micromech. Microeng. 25 (1) (2015) 015012.
[30] A.S. Savoia, G. Caliano, M. Pappalardo, A CMUT probe for medical ultrasonography: from microfabrication to system integration, IEEE Trans. Ultrason. Ferroelectr. Freq. Control 59 (6) (2012) 1127–1138.

Maëva Vallet was born in Nîmes, France, in 1988. She graduated from the engineering school Phelma (Grenoble INP) in Grenoble, France, in 2012 with a focus in physics and nanosciences and obtained her Ph.D. in 2015. Her Ph. D. research on photoacoustic imaging was realized in co-agreement between the Centre de Recherche en Acquisition et Traitement de l'Image pour la Santé (CREATIS), Lyon, France and the Laboratoire d'Imagerie et Systèmes d'Acquisition (LISA) of CEA-LETI, Grenoble, France. She is currently working as an R&D engineer in a biotech start-up in Cambridge, United Kingdom.

François Varray was born in Montpellier, France, in 1985. He received the Engineering Diploma and the master's degree in image and signal processing from the Ecole des Mines de Saint-Etienne, Saint-Etienne, France, in 2008, and the Ph.D. degree with a focus on nonlinear ultrasound simulation in 2011. His Ph.D. research was realized in co-agreement between the Centre de Recherche en Acquisition et Traitement de l'Image pour la Santé (CREATIS), Lyon, France and the MSD Laboratory, Florence, Italy. Since 2013, he has been an Associate Professor with CREATIS. His research interests include the nonlinear ultrasound propagation simulation, nonlinear image simulation, multi-resolution motion estimation, cardiac imaging, and photoacoustic imaging.

Dr. Jérôme Boutet, graduated as an engineer in Physics from Institut National Polytechnique de Grenoble (INPG). Then, he obtained a Ph.D. in Physics for Life Sciences from Grenoble University. After joining CEA-LETI, he became project manager and coordinator of the ANR-TECSAN PROSTAFLUO project which aimed to develop an optical probe to improve prostate cancer diagnostics. He is now project manager of project BITUM (Investissements d'avenir, call Nanobiotechnologies) on the same subject. These developments have led to the file of 17 patents and the publication of 18 papers, 1 book chapter and 8 reviewed proceedings.

Jean-Marc DINTEN is Senior Scientist at the Biology and Health Division in CEA-LETI. For more than 20 years, he has been widely developing medical image processing and reconstruction algorithms associated to the development of innovative X-Rays and Optical imaging systems. He now heads the Imaging Readout Systems Laboratory which develops new optical imaging systems for health and biology applications.

Giosuè Caliano received a M.S. degree in electronic engineering from the University of Salerno in 1993. After receiving the degree, he served as a postgraduate fellow in the Department of Electronics of the University of Salerno, both in didactic and research fields. His interests were in developing piezoelectric pressure sensors and in measurement techniques for ceramics' characteristics. In 1995, he joined Pirelli-FOS as an Industrial Automation Engineer. In this position, he worked as design engineer for optical fiber production. Since 1997, he has worked at the ACULAB, Department of Engineering, University Roma Tre, as head of the laboratory, and since 2012, he has been Adjunct Professor of "Sensors and Transducers". In 2014, he obtained the "National Academic Qualification" as Associate Professor in Electronics.
He is involved in design and characterization of micromachining ultrasonic transducers (CMUTs). In this position, he developed many types of CMUT transducers, from mono-element transducers to a 192-element probe for echographic imaging system. He obtained the first echographic images using a CMUT probe in conjunction with a commercial echographic system (2003), and he patented the new technology for CMUT fabrication called Reverse Process Technology. He is author of more than 110 papers on these fields published in international magazines and conference proceedings, plus 11 international patents. He was the founder of the International Workshop on CMUTs and has organized the event in 2001 (Roma), 2011 (Salerno), and 2016 (Roma). In 2009, he was the Local Chair of the 2009 IEEE International Ultrasonics Symposium, held in Rome.

Alessandro Stuart Savoia was born in Edinburgh, Scotland (UK), in 1978. He received the Laurea and the Ph.D. in Electronic Engineering from Università degli Studi Roma Tre, Rome, in 2003 and 2007, respectively. He has held a postdoctoral research position at the Department of Electronics Engineering of the same University since 2007. In the years 2008–2010 he participated, as a co-founder and R&D Manager, in an academic spin-off company of Roma Tre University in collaboration with the medical device company Esaote S.p.A., granted by the Italian Ministry of Education (MIUR), for the industrial exploitation of the scientific results on MEMS-based ultrasonic transducers (CMUTs), most of them achieved during his Ph.D. and Post-Doctoral research. In 2014, he became Assistant Professor in Electronics at the Department of Engineering of Roma Tre University. In 2017 he obtained the National Scientific Qualification (ASN) for Associate Professor in the scientific field "Electronics".
He has conducted research activity in the Acoustoelectronics Laboratory (ACULAB) mainly in the field of ultrasonic transducers and their applications. During his scientific career, he has focused on analytical and FEM modeling, design, microfabrication and packaging, characterization, electronics and system integration of MEMS-based Capacitive Micromachined Ultrasonic Transducers (CMUTs). His research interests also include piezoelectric ultrasonic transducers, and ultrasound beamforming and imaging techniques for medical and biometric applications.
Dr. Savoia has authored and co-authored about 60 papers in international journals and conferences, and three book chapters. He holds 4 international patents. He has carried out consultancy activities as a scientific advisor in the field of acousto-electronics for several semiconductor and medical device companies.

Didier Vray is currently a Professor of Signal Processing and Computer Sciences at INSA-Lyon, France. Since he joined the research laboratory CREATIS, his main research interest focus on ultrasound medical imaging. His research includes vascular imaging, flow imaging, tissue motion estimation, and bimodality US/Optics imaging. He is the author of more than 100 scientific publications and 2 issued patents in this field.